Dalton Transactions

COMMUNICATION

Cite this: *Dalton Trans.*, 2019, **48**, 17713

Received 12th November 2019,
Accepted 18th November 2019

DOI: 10.1039/c9dt04368c

rsc.li/dalton

Coordination-driven self-assembly of $M_{10}L_8$ metal–organic bi-capped square antiprisms with adaptable cavities†

Xue-Zhi Wang,[a,b] Meng-Ying Sun,[a,b] Ji Zheng,[a] Dong Luo,[a] Li Qi,[c] Xiao-Ping Zhou *[a] and Dan Li *[a]

A family of polyhedral metal-imidazolate cages based on the flexible bi-imidazole ligand L and Cu^{2+} ions have been synthesized and characterized, featuring an unusual $Cu_{10}L_8$ bicapped square antiprism structure (or Johnson solids, J_{17}) with an adaptable cavity. These metal–organic cages encapsulate anions, and they will expand or compress after they are filled with different-sized anions.

In a biologic process, an enzyme may change its shape to modulate its activity when it binds to a substrate.[1] This is a well-known induced-fit theory for molecular recognition in biology, proposed by Koshland in 1958.[2] Metal–organic cages (MOCs) are assembled from metal ions or metal clusters and polytopic organic ligands through coordination bonds and show varied cavities (*e.g.* hydrophobic or hydrophilic), and they are ideal models for mimicking enzymes.[3] A huge number of MOCs with varied structures and topologies (*e.g.* Platonic and Archimedean solids) have been successfully assembled by a careful choice of organic ligands, metal ions, and counter ions,[3a,4] exhibiting advanced functions (separation,[5] recognition and sensing,[6] stabilization of reactive species,[7] and catalysis,[3c,8] *etc.*). In these reported MOCs, rigid ligands are usually selected for the purpose of constructing robust architectures and probably circumventing the formation of dynamic mixtures of complexes in the complicated processes. However, in a biological system, an enzyme or protein is flexible and dynamic, which can adjust its conformation after being induced by a substrate to implement biologic functions. Therefore, learning from nature, the design and synthesis of flexible MOCs with adaptable cavities is an emergent technique and is significant. Limited examples of flexible MOCs with adaptable cavities have been reported.[9] Severin *et al.* showed that a hexanuclear Ru^{2+} based MOC can vary the size of its cavity from almost zero to more than 500 $Å^3$ by the encapsulation of two coronene molecules.[10] Clever *et al.* utilized light-mediated reactions to switch the cavity size of a Pd_2L_4 cage.[11] Nitschke *et al.* reported a $Fe^{II}_4L_4$ tetrahedron based on azaphosphatrane, which can structurally adapt its configurations in response to different sizes and shapes of anions in water.[12]

Coordination driven self-assembly of MOCs has witnessed tremendous advances in the past few decades. However, the formation of the predicted MOC with a defined structure from the assembly of multiple components is still a challenge, especially for a MOC with flexible ligands. For example, four distinct Cd^{II}-based architectures (a Cd_2L_3 helicate, a Cd_8L_{12} distorted cuboid, a $Cd_{10}L_{15}$ pentagonal prism, and a $Cd_{12}L_{18}$ hexagonal prism) are obtained by introducing different anionic templates,[13] while a series of gigantic MOCs ($M_{12}L_{24}$, $M_{24}L_{48}$, $M_{30}L_{60}$, and $M_{48}L_{96}$) were formed by slight changes in bending angles and the substituents of ligands and crystal growth temperatures.[14] A flexible ligand adopts varied conformations, thus serendipitous and unprecedented MOCs with unique structures are possibly formed during self-assembly.[15]

In our previous studies, we have successfully synthesized a series of rigid MOCs based on imidazole ligands by using the subcomponent self-assembly technology, including cubic, rhombic dodecahedral, and tetartoidal cages.[16] Here we report the coordination-driven self-assembly of four polyhedral metal-imidazolate cages based on a flexible ligand L and Cu^{2+} ions (Scheme 1), formulated as $[Cu_{10}L_8]\cdot nX$ (H_2L = *N*,*N*′-(propane-1,3-diyl)bis(1-(1*H*-imidazol-4-yl)methanimine), **1**, n = 4, X = ClO_4^-; **2**, n = 2, X = SiF_6^{2-}; **3**, n = 4, X = Br^-; **4**, n = 4, X = Cl^-). Cages **1–4** feature a bicapped square antiprism structure, which is rarely observed in MOCs. Interestingly, the cavity of

[a]*College of Chemistry and Materials Science, Jinan University, Guangzhou 510632, P. R. China. E-mail: zhouxp@stu.edu.cn, danli@jnu.edu.cn*
[b]*Department of Chemistry, Shantou University, Guangdong 515063, P. R. China*
[c]*Beijing National Laboratory of Molecular Sciences, Key Laboratory of Analytical Chemistry for Living Biosystems, Institute of Chemistry, Chinese Academy of Sciences, No. 2 Zhongguancun Beiyijie, Beijing 100190, P. R. China*

†Electronic supplementary information (ESI) available: Experimental details, supplementary structural figures, mass spectra, crystallographic data in CIF or other electronic formats, and computational details. CCDC Nos. 1866613–1866620. For ESI and crystallographic data in CIF or other electronic format see DOI: 10.1039/C9DT04368C

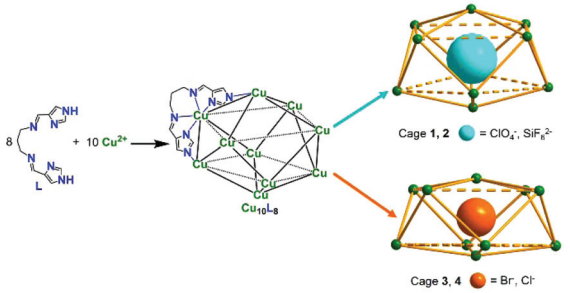

Scheme 1 Self-assembly of $Cu_{10}L_8$ metal–organic cages.

the bicapped square antiprism cage will expand after it is filled with big anions (*e.g.* ClO_4^-, SiF_6^{2-}) and obviously compress when small anions (*e.g.* Br^- and Cl^-) are introduced in comparison with that of the cage without an encapsulated anion, which was calculated by the DFT method. The host cavity volume alternates from 78 to 24 Å^3, revealing the high flexibility for this series of $Cu_{10}L_8$ cages. After exchanging the encapsulated guest anion, the expanded cage **1** can transform to the compressed cage **4**, ideally mimicking the 'induced-fit' process in a biological system.

Ligand H_2L was synthesized from the condensation of imidazole-4-carbaldehyde (2 equiv.) and 1,3-diaminopropane (1 equiv., for details see the ESI†). The successful formation of H_2L has been confirmed by ^{1}H NMR, ^{13}C NMR, and IR spectroscopies (see the ESI†). Cages **1–4** were synthesized by reacting H_2L with copper salts ($Cu(ClO_4)_2$), $CuSiF_6$, $CuBr_2$ and $CuCl_2$ for **1**, **2**, **3** and **4**, respectively) in mixture solvents under solvothermal conditions (for details, see the ESI†). Single crystals of cages **1–3** were obtained directly, while a powder product was obtained for cage **4**. However, reproducibility was poor for the synthesis of cage **2**, and the successful rate was about 10 percent. Single crystals of cage **4** could be obtained by the transformation from cage **1** through anion exchange under solvothermal conditions (see the ESI†).

Single crystal X-ray diffraction (SXRD) measurements revealed that cages **1–4** crystallize in the $P2_1/c$, $C2/c$, $P4/n$, and $P4/n$ space groups, respectively, featuring similar 10-nuclear metal-imidazolate cage structures (Fig. 1). Two types of Cu(II) ions exist in these cages. The first type (8 Cu(II) ions, denoted as Cu_e) is equatorial Cu(II) chelated by L, and the second type (2 Cu(II) ions, denoted as Cu_a) is axial Cu(II) bonded by 4 imidazolate ligands. The equatorial Cu(II) is five coordinated adopting a distorted square pyramidal geometry, while the axial Cu(II) can be treated as a five or six-coordinated ion (additional binding with anions or water molecules, see Fig. S1, ESI†). The Cu–N distances are similar in cages **1–4**, ranging from 1.979(5) to 2.201(4) Å. Each ligand contains two imidazolate groups and coordinates with three Cu(II) ions (Fig. S2, ESI†). In cages **1–4**, ten Cu(II) ions are bridged by 16 imidazolate groups to form a nanoscale $Cu_{10}L_8$ cage structure. Notably, in all cages, an anion (ClO_4^-, SiF_6^{2-}, Br^- or Cl^- in **1–4**, respectively) is encapsulated in the cavity of each corresponding cage (Fig. 1a–d). Careful analysis of the cage structure

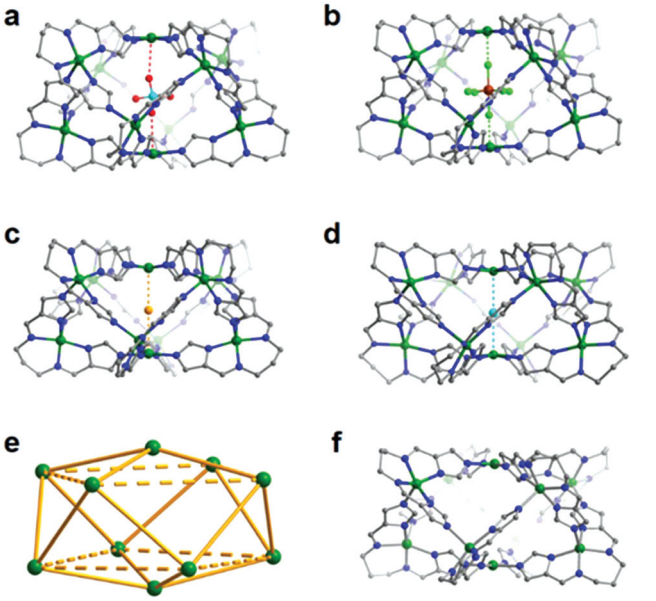

Fig. 1 Crystal structures of cage **1** (a), cage **2** (b), cage **3** (c), and cage **4** (d), the simplified topology of the cage (e), and DFT calculated cage **5** without encapsulated anions (f). Color codes: C grey, O red, N blue, F bright green, Cl cyan, Br light orange, Si brown, and Cu green. Hydrogens are omitted for clarity.

shows that the $Cu_{10}L_8$ cage can be simplified as a ball-stick structure by treating the Cu(II) ion as a ball and imidazolate groups as sticks (Fig. 1e). The rhombus windows of the cage are distorted, and the four vertices do not locate in the same plane. Thus, each rhombus window can be treated as two equilateral triangles, and the cage can be topologized as a hexadecahedron containing 10 vertices, 24 edges, and 16 equilateral triangles. This hexadecahedron shows a distorted gyroelongated square bipyramidal geometry, which is one of the Johnson solids, J_{17}. On the other hand, the cage structure can also be treated as a polyhedron by stacking two square pyramids with a square antiprism to form the *closo* bicapped square antiprism (Fig. S3, ESI†). The bicapped square antiprism geometry is known for metal clusters and the coordination geometry for rare earth metal ions (Fig. S4, ESI†).[17] It is not easy to construct a metal–organic bicapped square antiprism by design, since it requires metal ions with two types of coordination geometries and a unique ratio of 8 : 2. To the best of our knowledge, only one 40-nuclear MOC featuring a calixarene-based Johnson-type (J_{17}) structure has been reported.[18] Cages **1–4** represent serendipitous and unprecedented examples of metal–organic cages constructed from 10 metal ions and 8 flexible ligands with a special bicapped square antiprism or J_{17} structure.

Another typical feature of the $Cu_{10}L_8$ cage is its flexibility. Induced by the guest anions, the cage can expand and compress its cavity. The synthesis of a cage without filled anions is not successful. For a better understanding of how an anion affects a cage, a calculated $Cu_{10}L_8$ cage (denoted as **5**) model without encapsulated anions was optimized by using the DFT

Table 1 Internal volumes, $Cu_a\cdots Cu_a$ distances, and expanded ratios of MOCs and anion volumes

MOCs	Anions	Internal volume[a] (Å^3)	Anion volume[b] (Å^3)	$Cu_a\cdots Cu_a$ [c] (Å)	Expanded ratio[d]
1	ClO_4^-	76	55	7.801	+49%
2	SiF_6^{2-}	78	75	7.824	+53%
3	Br^-	28	26	5.788	−45%
4	Cl^-	24	22	5.466	−53%
5	Non.	51	Non	6.908	0

[a] Internal volumes were calculated by VOIDOO.[19] [b] The structures were optimized by the DFT method in Gaussian 09 and the volumes were calculated by using the Materials Studio software.[20] [c] $Cu_a\cdots Cu_a$ is the distance between two axial Cu(II) ions in the cage. [d] The expanded ratio is the differential internal volume of the as-synthesized cage and the calculated cage divided by the internal volume of the calculated cage. + meaning expansion, and − meaning compression.

method (Fig. 1f, for calculation details see the ESI†). As shown in Table 1, the internal volume of cage **5** is 51 Å^3, which is smaller than those of the expanded cage **1** (76 Å^3) and cage **2** (78 Å^3) and obviously larger than those of cage **3** (28 Å^3) and cage **4** (24 Å^3). As shown in Table 1, the expanded ratios for cages **1** and **2** are 49% and 53% respectively, and the compressed ratios for cages **3** and **4** are 45% and 53%, respectively. The Cl^- (being the smallest anion in this study) anion compresses the cage to its smallest internal volume in all instances. It is expected that the cage remains in a "relaxed" state when there is no inner anion and shows a moderate internal volume. The internal volume of cages **1**, **2**, **3**, and **4** is very close to the volume of the corresponding encapsulated anions (Table 1). The fully occupied anions in the cavities of the cages are due to the close multiple interactions between the anions and the cages (Fig. S5, ESI†), especially for cage **2**. In **2**, SiF_6^{2-} strongly coordinates with the Cu_a ions with short bond distances ranging from 2.172 to 2.278 Å and interacts with imidazolate groups through multiple F···H–C weak hydrogen bonds (H···F distances: 2.340 to 2.680 Å, Fig. S5b, ESI†). Thus, the encapsulated guest anions play a critical role in the conformational change for cages **1–4**, showing an excellent example of 'induced fit'.

Furthermore, to better understand the variation of the cage structures, each synthesized cage is overlaid with the calculated cage **5** by using the Materials Studio software to compare the conformation changes. As shown in Fig. S6, ESI,† compared with the calculated empty cage, cages **1** and **2** expand vertically (stretching along the axial copper centers), while cages **3** and **4** compress along the vertical direction. Thus, the $Cu_a\cdots Cu_a$ distances in cages **1** (7.801 Å) and **2** (7.824 Å) become longer after the cages are filled with relatively large ClO_4^- and SiF_6^{2-} anions, respectively, while those in cages **3** (5.788 Å) and **4** (5.466 Å) become obviously shorter after the cages are bound with small Br^- and Cl^- (Table 1, and Fig. S7, ESI†), respectively. These results are in good agreement with their internal volume changes (Table 1). Besides the $Cu_a\cdots Cu_a$ change, a slight change in the diagonal distances of $Cu_e\cdots Cu_e$ on the equatorial plane is also observed (Fig. 2). To know the

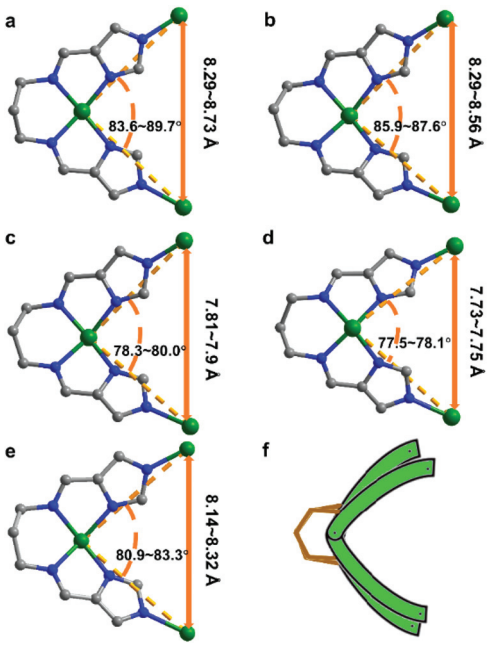

Fig. 2 The angles of <Cu–Cu–Cu and the distances of Cu–Cu in a Cu–L1 unit in cages **1** (a), **2** (b), **3** (c), **4** (d), and **5** (e), respectively. The simplified diagram of the hinged Cu–L unit (f). In the hinged Cu–L unit, the angles of <Cu–Cu–Cu range from 77.5 to 89.7°, and the distances for Cu–Cu range from 7.73 to 8.73 Å. Color codes: C grey, N blue, and Cu green.

mechanism of the highly flexible property of the $Cu_{10}L_8$ cage, a detailed structural analysis of cages **1–5** is carried out. Fig. 2 shows that the coordination of the equatorial Cu(II) ions is very flexible, benefiting from the dynamic properties of coordination bonds. The Cu–L unit is like a hinge, and the two binding imidazolate groups can rotate around the Cu(II) centers within a certain range (from 77.5 to 89.7°, Fig. 2). On the other hand, the ligand with the 1,3-propanediimine group is flexible, which does not constrain the variation of the geometry of the Cu(II) centers. Consequently, the flexible ligand and dynamic coordination bonds are responsible for the adaptive properties of these unique cages.

For comparison, we carefully checked our previously reported metal-imidazolate cages, which are also functionalized with Schiff-base groups. As shown in Fig. S8 (ESI†), although various anions (BF_4^-, ClO_4^-, PF_6^-, $CF_3SO_3^-$, NO_3^-, Br^-, and Cl^-) with different sizes are used for balancing the charge, the sizes of cages M_8L_6,[16c] $M_{14}L_{24}$,[16b] and $M_{20}L_{12}(OH)_{12}$[16d] do not change and the cages become rigid. This comparison indicates that cages **1–4** are unique with adaptive properties.

Anions can template the formation of metal–organic cages with varied structures.[6a,13,21] For example, perchlorate anions can induce the formation of a $Co_{10}L_{15}$ pentagonal prism, acting as a template anion.[6a] However, in this system, different-sized and shaped anions lead to the topologically same cage, indicating that the templating effect may not play a significant role. Furthermore, upon slightly changing the reac-

tion conditions, one dimensional zigzag coordination polymers are formed (compounds **5–8**, for synthesis and structures, see the ESI and Fig. S9†). This result further shows that the $Cu_{10}L_8$ MOCs are likely kinetic products in the crystallization process rather than being directed by the templating effect.

Mass spectrometry (MS) was used to check the $Cu_{10}L_8$ cage structure in solution. Cages **1–4** are soluble in polar organic solvents, such as *N*,*N*-dimethylformamide (DMF), methanol and acetonitrile. The high-resolution mass spectra of cages **1–4** were measured by using a trap-orbitrap mass spectrometer in acetonitrile. As shown in Fig. S10,† peaks at *m*/*z* = 835.7102 and 1330.0474 are visible in the spectrum of cage **1**, and correspond to $[(Cu_{10}L_8)\cdot ClO_4]^{3+}$ and $[(Cu_{10}L_8)\cdot 2ClO_4]^{2+}$, respectively. For cage **2**, the peak at *m*/*z* = 1301.0745 represents the composition of $[(Cu_{10}L_8)\cdot SiF_6]^{2+}$ (Fig. S10b†). Similar to cage **1**, two prominent peaks are observed at *m*/*z* = 847.0392 and 1310.5066 for cage **3** (Fig. S10c†), and they can be assigned to $[(Cu_{10}L_8)\cdot Br]^{3+}$ and $[(Cu_{10}L_8)\cdot 2Br]^{2+}$, respectively. Although the single crystal of cage **4** cannot be obtained by direct synthesis, similar to cages **1** and **3**, two prominent peaks are observed at *m*/*z* = 832.3781 and 1266.0524 (Fig. S10d†), respectively. These two peaks can be assigned to $[(Cu_{10}L_8)\cdot Cl]^{3+}$ and $[(Cu_{10}L_8)\cdot 2Cl]^{2+}$, respectively, showing that cage **4** has a similar $Cu_{10}L_8$ structure in solution to cages **1–3**. Moreover, the isotopic patterns of each resolved peak were in good agreement with the simulated patterns (Fig. S6 and S11–S13, ESI†), further demonstrating that MOCs **1–4** retain the $Cu_{10}L_8$ bicapped square antiprism structure in solution.

Due to the flexible and adaptive properties of the $Cu_{10}L_8$ bicapped square antiprisms, the compressed conformation and expanded conformation are possibly triggered by anion exchange. To test our hypothesis, cage **1** is chosen, due to its high yield and good solubility. An excess of KCl (0.2 mmol) was added to a CH_3CN solution (5.0 mL) of cage **1** (10.0 mg) at room temperature. After keeping at room temperature for 7 days, two new and weak peaks at *m*/*z* = 831.7333 and 1298.0645 belonging to $[(Cu_{10}L_8)\cdot Cl]^{3+}$and $[(Cu_{10}L_8)\cdot Cl\cdot ClO_4]^{2+}$, respectively, appeared in the mass spectra (Fig. S14, ESI†). The MS study indicates that the conversion of cage by anion exchange is possible but slow at room temperature. To enhance the exchange rate, drastic reaction conditions were used. The exchange reaction was carried out in a DMF/MeOH solution under solvothermal conditions (100 °C, 3 days). Fortunately, dark-green block crystals were obtained after the reaction (Fig. 3a), and they are different from the green rhombohedron-like single crystal of cage **1**. The SXRD study revealed that the transformed product features a $Cu_{10}L_8$ bicapped square antiprism structure encapsulating a Cl^- anion (Fig. 1d), which unambiguously confirms the successful transformation from cage **1** to cage **4**. Interestingly, the internal volume and $Cu_a\cdots Cu_a$ distance change from 76 $Å^3$ and 7.801 Å to 24 $Å^3$ and 5.466 Å, respectively, after transformation (Table 1, and Fig. 2), indicating that the adaptive cage transforms from the expanded conformation to the compressed conformation, induced by the Cl^- anion. The mass

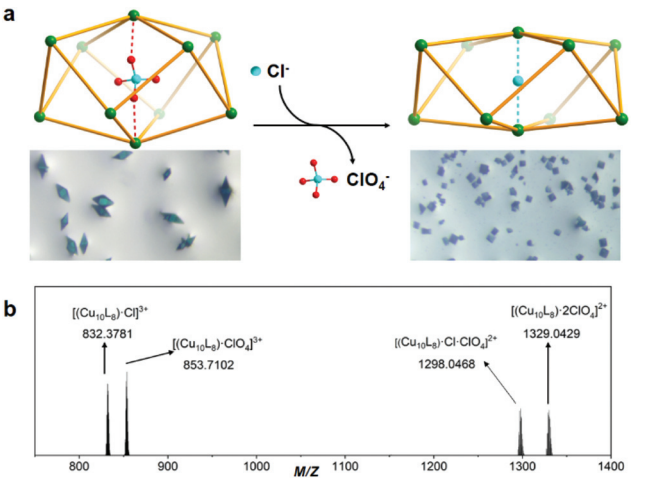

Fig. 3 The schematic representation of transforming cage **1** to cage **4** by exchanging ClO_4^- with Cl^-, and crystal photos of **4** and **1**, respectively (a). The mass spectrum of the transformed product (b).

spectrum of the product shows that the transformation of cage **1** to cage **4** is not fully completed (Fig. 3b and Fig. S15, ESI†). The possible reason for this is that the windows of cage **1** are small (Fig. S16, ESI†), which makes the free exchange between ClO_4^- and Cl^- difficult. Furthermore, trials to transform the compressed cage **3** or **4** to the expanded cage **1** were not successful.

In summary, a series of $Cu_{10}L_8$ MOCs have been successfully synthesized and characterized. These MOCs show unusual metal–organic bicapped square antiprism structures and are highly flexible with adaptive cavities. Crystallographic analysis and DFT calculations revealed that the $Cu_{10}L_8$ MOC can undergo 'induced fit' to bind guest anions. In comparison with the calculated cage, the internal volume of the synthesized MOC can expand and compress more than 53% to encapsulate a wide range of anions. Of particular interest is the expanded ClO_4^--bound cage, which can transform to the highly compressed Cl^--bound one. These flexible MOCs provide typical 'induced fit' examples for mimicking enzymes. Further work will seek to make luminescent cages with the function of 'induced fit' to effectively sense anions.

Conflicts of interest

There are no conflicts to declare.

Acknowledgements

This work was financially supported by the National Natural Science Foundation of China (No. 21731002, 21975104, 21871172 and 21371113), the Guangdong Natural Science Funds for Distinguished Young Scholar (2014A030306042), and Jinan University.

Notes and references

1 D. D. Boehr, R. Nussinov and P. E. Wright, *Nat. Chem. Biol.*, 2009, **5**, 789.

2 D. E. Koshland, *Proc. Natl. Acad. Sci. U. S. A.*, 1958, **44**, 98–104.

3 (*a*) S. R. Seidel and P. J. Stang, *Acc. Chem. Res.*, 2002, **35**, 972–983; (*b*) M. J. Wiester, P. A. Ulmann and C. A. Mirkin, *Angew. Chem., Int. Ed.*, 2011, **50**, 114–137; (*c*) D. M. Kaphan, M. D. Levin, R. G. Bergman, K. N. Raymond and F. D. Toste, *Science*, 2015, **350**, 1235–1238; (*d*) A. J. McConnell, C. S. Wood, P. P. Neelakandan and J. R. Nitschke, *Chem. Rev.*, 2015, **115**, 7729–7793.

4 (*a*) M. Fujita, M. Tominaga, A. Hori and B. Therrien, *Acc. Chem. Res.*, 2005, **38**, 369–378; (*b*) M. M. J. Smulders, I. A. Riddell, C. Browne and J. R. Nitschke, *Chem. Soc. Rev.*, 2013, **42**, 1728–1754; (*c*) K. Byrne, M. Zubair, N. Zhu, X.-P. Zhou, D. S. Fox, H. Zhang, B. Twamley, M. J. Lennox, T. Düren and W. Schmitt, *Nat. Commun.*, 2017, **8**, 15268.

5 (*a*) W. Xuan, M. Zhang, Y. Liu, Z. Chen and Y. Cui, *J. Am. Chem. Soc.*, 2012, **134**, 6904–6907; (*b*) K. Wu, K. Li, Y. J. Hou, M. Pan, L. Y. Zhang, L. Chen and C. Y. Su, *Nat. Commun.*, 2016, **7**, 10487; (*c*) C. Garcia-Simon, M. Garcia-Borras, L. Gomez, T. Parella, S. Osuna, J. Juanhuix, I. Imaz, D. Maspoch, M. Costas and X. Ribas, *Nat. Commun.*, 2014, **5**, 5557.

6 (*a*) I. A. Riddell, M. M. J. Smulders, J. K. Clegg, Y. R. Hristova, B. Breiner, J. D. Thoburn and J. R. Nitschke, *Nat. Chem.*, 2012, **4**, 751–756; (*b*) W. Meng, B. Breiner, K. Rissanen, J. D. Thoburn, J. K. Clegg and J. R. Nitschke, *Angew. Chem., Int. Ed.*, 2011, **50**, 3479–3483; (*c*) C.-L. Liu, R.-L. Zhang, C.-S. Lin, L.-P. Zhou, L.-X. Cai, J.-T. Kong, S.-Q. Yang, K.-L. Han and Q.-F. Sun, *J. Am. Chem. Soc.*, 2017, **139**, 12474–12479.

7 P. Mal, B. Breiner, K. Rissanen and J. R. Nitschke, *Science*, 2009, **324**, 1697–1699.

8 (*a*) C. Tan, J. Jiao, Z. Li, Y. Liu, X. Han and Y. Cui, *Angew. Chem., Int. Ed.*, 2018, **57**, 2085–2090; (*b*) X. Jing, C. He, Y. Yang and C. Duan, *J. Am. Chem. Soc.*, 2015, **137**, 3967–3974; (*c*) M. D. Pluth, R. G. Bergman and K. N. Raymond, *Acc. Chem. Res.*, 2009, **42**, 1650–1659.

9 (*a*) S. Loffler, J. Lubben, L. Krause, D. Stalke, B. Dittrich and G. H. Clever, *J. Am. Chem. Soc.*, 2015, **137**, 1060–1063; (*b*) F. J. Rizzuto and J. R. Nitschke, *Nat. Chem.*, 2017, **9**, 903.

10 S. Mirtschin, A. Slabon-Turski, R. Scopelliti, A. H. Velders and K. Severin, *J. Am. Chem. Soc.*, 2010, **132**, 14004–14005.

11 M. Han, R. Michel, B. He, Y.-S. Chen, D. Stalke, M. John and G. H. Clever, *Angew. Chem., Int. Ed.*, 2013, **52**, 1319–1323.

12 D. Zhang, T. K. Ronson, J. Mosquera, A. Martinez, L. Guy and J. R. Nitschke, *J. Am. Chem. Soc.*, 2017, **139**, 6574–6577.

13 I. A. Riddell, T. K. Ronson, J. K. Clegg, C. S. Wood, R. A. Bilbeisi and J. R. Nitschke, *J. Am. Chem. Soc.*, 2014, **136**, 9491–9498.

14 (*a*) S. Sato, J. Iida, K. Suzuki, M. Kawano, T. Ozeki and M. Fujita, *Science*, 2006, **313**, 1273–1276; (*b*) Q. F. Sun, J. Iwasa, D. Ogawa, Y. Ishido, S. Sato, T. Ozeki, Y. Sei, K. Yamaguchi and M. Fujita, *Science*, 2010, **328**, 1144–1147; (*c*) D. Fujita, Y. Ueda, S. Sato, N. Mizuno, T. Kumasaka and M. Fujita, *Nature*, 2016, **540**, 563–566; (*d*) D. Fujita, Y. Ueda, S. Sato, H. Yokoyama, N. Mizuno, T. Kumasaka and M. Fujita, *Chem*, 2016, **1**, 91–101.

15 M. D. Ward, *Chem. Commun.*, 2009, 4487–4499.

16 (*a*) X.-P. Zhou, J. Liu, S.-Z. Zhan, J.-R. Yang, D. Li, K.-M. Ng, R. W.-Y. Sun and C.-M. Che, *J. Am. Chem. Soc.*, 2012, **134**, 8042–8045; (*b*) X.-P. Zhou, Y. Wu and D. Li, *J. Am. Chem. Soc.*, 2013, **135**, 16062–16065; (*c*) D. Luo, X.-P. Zhou and D. Li, *Angew. Chem., Int. Ed.*, 2015, **54**, 6190–6195; (*d*) D. Luo, X.-Z. Wang, C. Yang, X.-P. Zhou and D. Li, *J. Am. Chem. Soc.*, 2018, **140**, 118–121.

17 (*a*) C. Liu, L.-J. Li, X. Jin, J. E. McGrady and Z.-M. Sun, *Inorg. Chem.*, 2018, **57**, 3025–3034; (*b*) T. Kajiwara, M. Nakano, S. Takaishi and M. Yamashita, *Inorg. Chem.*, 2008, **47**, 8604–8606.

18 X. Hang, B. Liu, X. Zhu, S. Wang, H. Han, W. Liao, Y. Liu and C. Hu, *J. Am. Chem. Soc.*, 2016, **138**, 2969–2972.

19 G. J. Kleywegt and T. A. Jones, *Acta Crystallogr., Sect. D: Biol. Crystallogr.*, 1994, **50**, 178–185.

20 M. J. Frisch, G. W. Trucks, H. B. Schlegel, *et al.*, *Gaussian 09 (Revision E.01)*, Gaussian Inc., Wallingford, CT, 2013.

21 R. Custelcean, P. V. Bonnesen, N. C. Duncan, X. Zhang, L. A. Watson, G. Van Berkel, W. B. Parson and B. P. Hay, *J. Am. Chem. Soc.*, 2012, **134**, 8525–8534.